

Optomechanical Coupling in a Two-Dimensional Photonic Crystal Defect Cavity

E. Gavartin,¹ R. Braive,^{2,3} I. Sagnes,² O. Arcizet,⁴ A. Beveratos,² T. J. Kippenberg,^{1,5,*} and I. Robert-Philip^{2,†}

¹*Ecole Polytechnique Fédérale de Lausanne, EPFL, 1015 Lausanne, Switzerland*

²*Laboratoire de Photonique et de Nanostructures, Route de Nozay, 91460 Marcoussis, France*

³*Université Paris Denis Diderot, 75205 Paris, Cedex 13, France*

⁴*Institut Néel, 25 rue des Martyrs, 38042 Grenoble, France*

⁵*Max Planck Institut für Quantenoptik, 85748 Garching, Germany*

(Received 29 November 2010; revised manuscript received 3 April 2011; published 17 May 2011)

Periodically structured materials can sustain both optical and mechanical modes. Here we investigate and observe experimentally the optomechanical properties of a conventional two-dimensional suspended photonic crystal defect cavity with a mode volume of $\sim 3(\lambda/n)^3$. Two families of mechanical modes are observed: flexural modes, associated to the motion of the whole suspended membrane, and localized modes with frequencies in the GHz regime corresponding to localized phonons in the optical defect cavity of diffraction-limited size. We demonstrate direct measurements of the optomechanical vacuum coupling rate using a frequency calibration technique. The highest measured values exceed 80 kHz, demonstrating high coupling of optical and mechanical modes in such structures.

DOI: 10.1103/PhysRevLett.106.203902

PACS numbers: 42.70.Qs, 43.40.Dx

Cavity optomechanics [1] exploits the coupling of mechanical oscillators to the light field via radiation pressure. On the applied side, such coupling may be used to enable novel radiation pressure driven clocks [2], make highly sensitive displacement sensors, tunable optical filters [3], delay lines [4,5] or enable photon storage on a chip using optomechanically induced transparency [5,6]. On a fundamental level, such systems can be exploited for demonstrating that nano- and micromechanical oscillators can exhibit quantum mechanical behavior [7]. Among various submicron optomechanical systems presently investigated [8], suspended membranes containing a photonic crystal cavity offer strong light confinement in diffraction-limited volumes and are therefore natural candidates for achieving high optomechanical coupling. Recently, optomechanical coupling in 1D photonic crystal systems [9] has been observed in patterned single [10] and dual nanobeams (zipper cavities) [11,12]. It would be highly desirable to extend such optomechanical coupling to 2D systems, notably photonic crystal defect cavities. Such cavities offer strong light confinement (i.e., small mode volume), high quality factors (Q) [13] and have been used for studying cavity QED using quantum dots [14] or for realizing nanolasers [15,16]. Recently, a 2D optomechanical photonic crystal slot cavity has been reported [17]. While mechanical displacement due to strong radiation force generated by band-edge modes in bilayer photonic crystal slabs has been reported as well [18], to date optomechanical coupling of the 2D conventional defect cavity has not been studied.

In this Letter, we demonstrate optomechanical coupling using a photonic crystal defect ($L3$) cavity. We provide a direct and robust experimental determination of the vacuum optomechanical coupling rate [19] using frequency modulation, showing a particularly high coupling for the

localized mechanical modes, which may also be coupled to quantum dots in future studies [20].

The optomechanical device under study consists of a 262 nm thick InP suspended membrane containing a two-dimensional photonic crystal defect cavity shown in Fig. 1(a). The cavity, following the design proposed in [13], contains three missing holes in a line of a perfect triangular lattice of holes with a lattice constant of $a = 430$ nm and a radius $r = 90$ nm. At both edges of the cavity the holes are displaced outwards by $d = 0.18a$, in order to obtain high optical quality factors. The cavity is fabricated using electron beam lithography, inductively coupled plasma etching [21], and wet etching. It incorporates a single layer of self-assembled InAsP quantum dots [22] at its vertical center plane for cavity characterization. The presence of the dots inside the cavity allows us to identify the spectral properties of the fundamental optical mode of the cavity by photoluminescence measurements [23], as shown in Fig. 1(b). The resonance wavelength of the fundamental mode is centered around 1555 nm and the cold-cavity quality factor is measured to be $\sim 10^4$ (cavity linewidth is $\kappa/2\pi \approx 20$ GHz). The suspended photonic crystal membrane lies on top of a 10 μm high mesa structure [see Fig. 1(a)]. The mesa structure is processed to enable positioning of a tapered optical fiber in the evanescent field of the cavity, while precluding any interaction with the nearby substrate. The shape of the membrane resembles a Bezier curve.

The setup used in the experiment is depicted in Fig. 1(d). An external-cavity diode laser is used for the readout of the mechanical motion. Coupling to the optical modes of the suspended membrane is achieved with the optical fiber-taper technique [24]. Piezoelectric actuators enable an accurate positioning allowing us to optimize the gap

between the fiber-taper and the defect cavity, and thus to increase evanescent coupling. Despite careful reduction of the taper-cavity gap, only a small fraction of the light can be coupled into the defect cavity, typically not exceeding 10% of the incoming laser power. The cavity-fiber system is kept in a vacuum chamber with a pressure below 1 mbar. Laser light coupled inside the photonic crystal cavity leads to local heating, which induces a thermal effect arising from the temperature dependent refractive index n [25]. As $dn/dT > 0$ (T is the temperature) for InP [26], the region detuned to the blue side of the resonance allows thermal passive locking [25]. In our experiments the laser frequency is chosen to correspond to the blue-detuned side of the fringe of the optical mode requiring no further locking. Mechanical motion of the membrane is imprinted on the transmitted optical intensity through modulation of the internal cavity field. An electro-optical modulator is used for frequency modulation to determine the optomechanical coupling rate. The transmitted signal is detected by a fast receiver and the electrical signal is analyzed with an oscilloscope as well as an electronic spectrum analyzer.

For a launched laser power of 1.3 mW more than 20 mechanical modes are observed in the frequency range between 10 MHz and 1 GHz. These modes can be separated into two mode families. The first family consists of flexural modes present in the low-frequency range (below 200 MHz), whereas the second family consists of localized modes. Flexural modes, whose spectrum is shown in Fig. 2(a), are characterized by displacement patterns distributed over the entire membrane. They can be interpreted as drum modes, whose specific displacement patterns are subject to the specific geometry and clamping

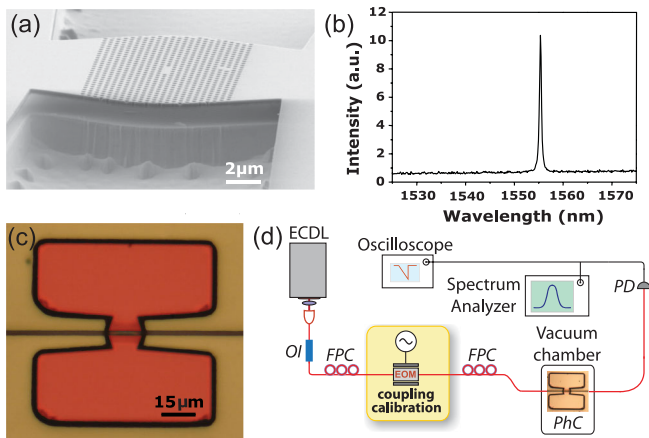


FIG. 1 (color). (a) Scanning electron microscope side view of the cavity. (b) Microphotoluminescence spectrum of the photonic crystal slab cavity obtained under nonresonant continuous optical excitation at normal incidence with an excitation power of $100 \mu\text{W}$ at 532 nm . (c) Micrograph (false colors) of a defect cavity-fiber taper system used to read out mechanical motion of the cavity. (d) Experimental setup (ECDL: External-cavity diode laser, OI: optical isolator, EOM: electro-optical modulator, FPC: fiber polarization controller, PhC: photonic crystal defect cavity, PD: photodiode).

conditions of the membrane. In order to identify the various modes, we modeled the mechanical properties of the photonic crystal slab structure by finite element modeling. Realistic geometry parameters were taken into account, including the under-etching of the mesa structures between which the membrane is suspended. A good agreement between measurements and modeling is obtained using a Young modulus of 20 GPa (slightly smaller than usual values observed in bulk InP materials [27] attributed to the perforation for the photonic crystal). Figure 2(b) shows the displacement patterns of the first five modes as well as a prominent mode around 150 MHz.

Localized modes, shown in Fig. 3(a), correspond to mechanical displacement of the membrane localized in the cavity core of the defect. We were able to resolve the fundamental localized mode at 0.46 GHz as well as the three higher orders (at 0.72 , 0.99 , and 1.26 GHz). The inset of Fig. 3(a) compares the simulated against the measured resonance frequencies of the mechanical modes that could be assigned, revealing excellent agreement both for flexural and localized modes. The progression of the resonance frequency of the localized modes versus mode number is shown in Fig. 3(c) and follows a linear behavior with mode number.

Importantly, localized mechanical modes coincide spatially fully with the optical defect cavity mode. Therefore, the photonic crystal not only offers strong optical confinement, but simultaneously high phonon confinement. We

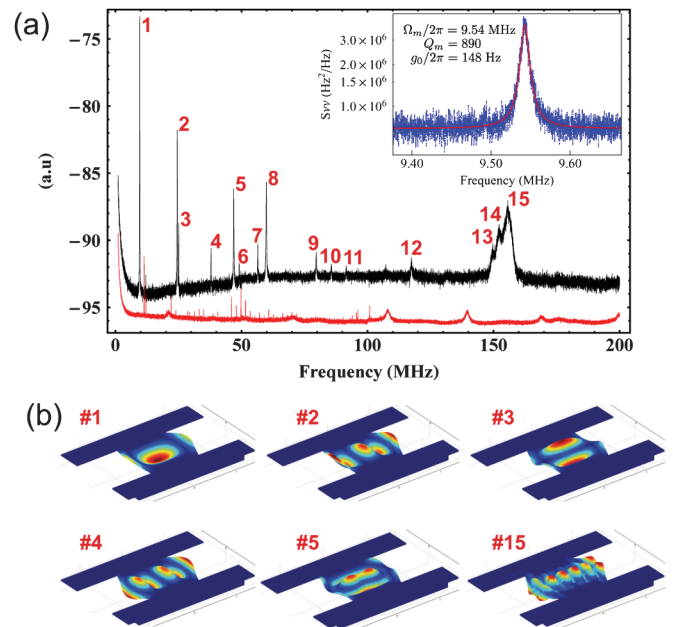


FIG. 2 (color). (a) Detected frequency noise spectrum in the 1 MHz–200 MHz range presenting a series of peaks corresponding to the different mechanical modes labeled by numbers (Black curve). The red curve represents a spectrum acquired with the laser being detuned out of resonance. Inset: Calibrated frequency noise spectrum of the fundamental mode (#1) with a Lorentzian fit (red line). (b) Spatial displacement patterns of exemplary six mechanical modes, as obtained from finite element modeling.

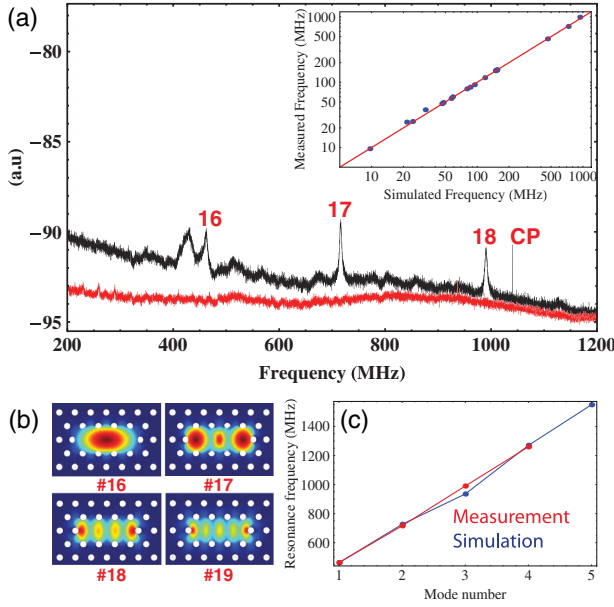


FIG. 3 (color). (a) Detected frequency noise spectrum in the 200 MHz–1.2 GHz range presenting a series of peaks corresponding to the different mechanical modes with the localized modes labeled by numbers (Black curve). The mode on the left of the first order localized mode could not be identified through simulations. The red curve represents a spectrum acquired with the laser being detuned out of resonance. CP denotes the calibration peak resulting from the frequency modulation measurement. Inset: Measured versus simulated frequency for mechanical modes which could be accurately identified (#1–19). (b) Spatial displacement pattern for the first four orders of localized mechanical modes, as obtained from finite element modeling. (c) Simulated (blue) and experimentally determined (red) progression of the resonance frequency of the localized modes versus mode number (mode #19 was determined in a separate measurement).

emphasize that the localization occurs in the absence of a phononic band gap [28]. Because of the colocalization of the optical and mechanical mode within the defect cavity, a high overlap of the mechanical displacement with the distribution of electromagnetic energy is expected which promises high optomechanical coupling. This is visualized in Fig. 4(a), where the results of the mechanical FEM simulation for the third order localized mode are compared with the spatial distribution of the electromagnetic field of the optical defect mode, which was obtained through a finite difference time-domain (FDTD) simulation. In a second experiment we determined the coupling rate for various flexural modes and the second and third order localized modes.

Usually, the optomechanical coupling strength is determined by two parameters—the optomechanical coupling parameter $G = \frac{d\omega_c}{dx}$, with ω_c being the resonance frequency of the optical resonator and x denoting the displacement of the mechanical oscillator, and the effective mass m_{eff} [29] of the mechanical mode. The necessity of introducing the effective mass routinely arises from the arbitrary choice of x . Particularly for photonic crystals it is

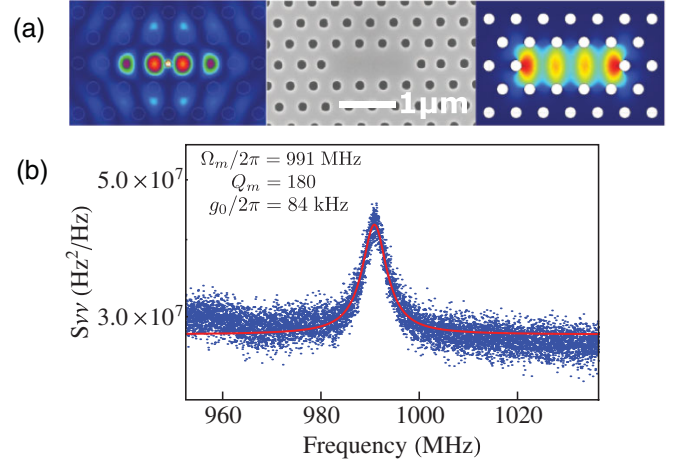


FIG. 4 (color). (a) Simulated distribution of the electromagnetic field (left), scanning electron microscope image of the defect (middle) and simulated third order localized mechanical mode (right). (b) Calibrated frequency noise spectrum of the third order localized mechanical mode #18 (blue points) with a Lorentzian fit (red line). A vacuum optomechanical rate of $g_0/2\pi = 84$ kHz is determined.

difficult to define an unambiguous displacement direction of a mechanical mode. Recently, it was suggested that the vacuum optomechanical coupling rate g_0 would be a more proper quantity to experimentally characterize optomechanical systems [19,30], as expected from the Hamiltonian description of the interaction (i.e., $\hat{H}_{\text{int}} = \hbar(Gx_{\text{zpf}})(\hat{a}_m + \hat{a}_m^\dagger)\hat{a}_p^\dagger\hat{a}_p$, where \hat{a}_m and \hat{a}_p are the phonon and photon annihilation operators, and $x_{\text{zpf}} = \sqrt{\hbar/2m_{\text{eff}}\Omega_m}$ denotes the zero-point fluctuations of the mechanical oscillator (\hbar represents the reduced Planck constant and $\Omega_m/2\pi$ the mechanical resonance frequency). In analogy to cavity Quantum Electrodynamics (cQED), g_0 is defined as $g_0 = G \cdot x_{\text{zpf}}$. As all relevant optomechanical parameters can be derived through knowledge of g_0 , acquiring its value would make the determination of G and m_{eff} redundant. As described in [19], the value g_0 can be determined experimentally via $g_0 = \sqrt{S_{\omega\omega}(\Omega_m)\frac{\Gamma_m}{4\bar{n}}}$, with \bar{n} being the average phonon occupancy of the mechanical mode, $\Gamma_m/2\pi$ being the mechanical damping rate and $S_{\omega\omega}(\Omega_m)$ being the frequency spectral density of cavity frequency noise evaluated at the mechanical resonance frequency. For high phonon occupancy one can approximate $\bar{n} \approx k_B T/\hbar\Omega_m \gg 1$, with k_B as Boltzmann's constant. $S_{\omega\omega}(\Omega_m)$ can be experimentally determined by a frequency modulation technique [31].

We performed a measurement of the cavity frequency noise by applying a known phase modulation to the laser using an LiNbO₃ electro-optical modulator (cf. Fig. 1). The modulation frequency was chosen to be close to the resonance frequency of the mechanical mode to be calibrated. The measurement also allows calibration of the frequency noise produced by the mechanical mode. A detailed

TABLE I. Optomechanical vacuum coupling rates for various modes determined experimentally via the frequency modulation technique.

Mode index	Measured frequency $\Omega_m/2\pi$ (MHz)	Measured vacuum coupling rate $g_0/2\pi$ (kHz)
1	9.54	0.15
2	24.45	0.40
5	46.87	1.28
8	59.83	3.96
17	716	71.6
18	991	83.8

account of the calibration method is given in [32]. A calibrated frequency noise spectrum for the fundamental flexural mode is shown in the inset of Fig. 2(a), and the optomechanical vacuum coupling rate was determined to be $g_0/2\pi = 148$ Hz. The mechanical quality factor for this mode is $Q_m = 890$ being the highest for all flexural modes. The coupling rate for the flexural modes increases with the mode number up to several kHz. The optomechanical coupling for the localized mechanical modes was determined to be $g_0/2\pi = 71.6$ kHz ($Q_m = 160$) and $g_0/2\pi = 83.8$ kHz ($Q_m = 180$) for the second and third order, respectively. A calibrated frequency noise spectrum for third order localized mode is shown in Fig. 4(b). The high values of $g_0/2\pi$ give a definite experimental proof of the high optomechanical coupling between a photonic crystal defect cavity and a localized mechanical mode. These coupling values are almost two orders of magnitudes higher than measured in whispering gallery mode (WGM) toroidal resonators [33] and doubly-clamped strained silicon nitride beams in the near field of a silica toroidal resonator [8], both of which are ca. $g_0/2\pi \approx 1$ kHz. Recently, an optomechanical system consisting of small-sized GaAs disks was introduced [34], which due to its size also allows an increased confinement of both optical and mechanical modes. Like in the system studied here this leads to a high mode overlap increasing optomechanical coupling to values of g_0 up to several kHz, albeit with possibility of improvement. The values of $g_0/2\pi$ which could be unambiguously obtained are specified in Table I.

The high coupling of the localized modes is promising for various applications. For example, by integrating a single quantum dot in the defect cavity, a multitude of experiments can be envisioned such as laser cooling [20] and coupling of a quantum mechanical oscillator to an artificial atom, once the ground state of the mechanical oscillator is reached. Moreover, the present planar architecture can be used for photon-phonon conversion experiments [4,5].

Funding for this work was provided by European NanoSci-ERA project NanoEPR, through QNEMS and MINOS by the FP7, the NCCR Quantum Photonics, the SNF and through an ERC Starting Grant SiMP.

*tobias.kippenberg@epfl.ch

†isabelle.robort@lpm.cnrs.fr

- [1] T.J. Kippenberg and K.J. Vahala, *Science* **321**, 1172 (2008); F. Marquardt and S.M. Girvin, *Physics* **2**, 40 (2009); I. Favero and K. Karrai, *Nat. Photon.* **3**, 201 (2009).
- [2] T.J. Kippenberg *et al.*, *Phys. Rev. Lett.* **95**, 033901 (2005); T. Carmon *et al.*, *ibid.* **94**, 223902 (2005).
- [3] J. Rosenberg *et al.*, *Nat. Photon.* **3**, 478 (2009); G.S. Wiederhecker *et al.*, *Nature (London)* **462**, 633 (2009).
- [4] A.H. Safavi-Naeini and O. Painter, *New J. Phys.* **13** 013017 (2011).
- [5] S. Weis *et al.*, *Science* **330**, 1520 (2010).
- [6] D. Chang *et al.*, *arXiv:1006.3529*.
- [7] K. Schwab and M. Roukes, *Phys. Today* **58**, 36 (2005).
- [8] J.D. Thompson *et al.*, *Nature (London)* **452**, 72 (2008); G. Anetsberger *et al.*, *Nature Phys.* **5**, 909 (2009); M. Li *et al.*, *Nature (London)* **456**, 480 (2008).
- [9] J. Foresi *et al.*, *Nature (London)* **390**, 143 (1997).
- [10] M. Eichenfield *et al.*, *Nature (London)* **462**, 78 (2009).
- [11] M. Eichenfield *et al.*, *Nature (London)* **459**, 550 (2009).
- [12] M. Eichenfield *et al.*, *Opt. Express* **17**, 20078 (2009).
- [13] Y. Akahane *et al.*, *Nature (London)* **425**, 944 (2003).
- [14] T. Yoshie *et al.*, *Nature (London)* **432**, 200 (2004).
- [15] O. Painter *et al.*, *Science* **284**, 1819 (1999).
- [16] S. Strauf *et al.*, *Phys. Rev. Lett.* **96**, 127404 (2006).
- [17] A.H. Safavi-Naeini *et al.*, *Appl. Phys. Lett.* **97**, 181106 (2010).
- [18] Y.-G. Roh *et al.*, *Phys. Rev. B* **81**, 121101(R) (2010).
- [19] M.L. Gorodetsky *et al.*, *Opt. Express* **18**, 23236 (2010).
- [20] I. Wilson-Rae, P. Zoller, and A. Imamoglu, *Phys. Rev. Lett.* **92**, 075507 (2004).
- [21] A. Talneau *et al.*, *Appl. Phys. Lett.* **92**, 061105 (2008).
- [22] A. Michon *et al.*, *J. Appl. Phys.* **104**, 043504 (2008).
- [23] R. Hosten *et al.*, *Opt. Lett.* **35**, 1154 (2010).
- [24] M. Cai, O. Painter, and K.J. Vahala, *Phys. Rev. Lett.* **85**, 74 (2000).
- [25] T. Carmon, L. Yang, and K. Vahala, *Opt. Express* **12**, 4742 (2004).
- [26] P. Martin *et al.*, *Appl. Phys. Lett.* **67**, 881 (1995).
- [27] <http://www.ioffe.ru/SVA/NSM/Semicond/InP/mechanic.html>.
- [28] M. Maldovan and E.L. Thomas, *Appl. Phys. Lett.* **88**, 251907 (2006).
- [29] A. Gillespie and F. Raab, *Phys. Rev. D* **52**, 577 (1995); M. Pinard, Y. Hadjar, and A. Heidmann, *Eur. Phys. J. D* **7**, 107 (1999).
- [30] A.H. Safavi-Naeini and O. Painter, *Opt. Express* **18**, 14926 (2010).
- [31] A. Schliesser *et al.*, *New J. Phys.* **10**, 095015 (2008).
- [32] See supplemental material at <http://link.aps.org/supplemental/10.1103/PhysRevLett.106.203902> for a detailed description.
- [33] A. Schliesser *et al.*, *Nature Phys.* **4**, 415 (2008).
- [34] L. Ding *et al.*, *Phys. Rev. Lett.* **105**, 263903 (2010).